Longitudinal and transverse NMR relaxivities of Ln(III)-DOTA complexes: A comprehensive investigation

Davide Cicolari, Fabio Santanni, Leonardo Grassi, et al.

View Online   Export Citation   CrossMark

ARTICLES YOU MAY BE INTERESTED IN

AIP Publishing

155, 214201

Longitudinal and transverse NMR relaxivities of Ln(III)-DOTA complexes: A comprehensive investigation

Davide Cicolari,[1,2,a] (iD) Fabio Santanni,[3] (iD) Leonardo Grassi,[3] (iD) Francesca Brero,[1,2] (iD) Marta Filibian,[2,4] (iD) Teresa Recca,[4] (iD) Paolo Arosio,[5,6] (iD) Mauro Perfetti,[3] (iD) Manuel Mariani,[1,2] (iD) Roberta Sessoli,[3] (iD) and Alessandro Lascialfari[1,2] (iD)

AFFILIATIONS

[1] Department of Physics, University of Pavia, Via Bassi 6, Pavia (PV) 27100, Italy
[2] INFN, Istituto Nazionale di Fisica Nucleare–Pavia Unit, Via Bassi 6, Pavia (PV) 27100, Italy
[3] Department of Chemistry, University of Florence, Sesto Fiorentino (FI) 50019, Italy
[4] Centro Grandi Strumenti, University of Pavia, Via Bassi 21, Pavia (PV) 27100, Italy
[5] Department of Physics, University of Milan, Via Celoria 16, Milan (MI) 20133, Italy
[6] INFN, Istituto Nazionale di Fisica Nucleare–Milan Unit, Via Celoria 16, Milan (MI) 20133, Italy

[a] Author to whom correspondence should be addressed: davide.cicolari01@universitadipavia.it. **Telephone:** +39 0382 987483

ABSTRACT

Longitudinal and transverse ^1H nuclear magnetic resonance relaxivities of Ln(III)-DOTA complexes (with Ln = Gd, Tb, Dy, Er; DOTA = 1,4,7,10-tetraazacyclododecane-N,N′,N″,N‴-tetraacetic acid) and Mn(II) aqueous solutions were measured in a wide range of frequencies, 10 kHz to 700 MHz. The experimental data were interpreted by means of models derived from the Solomon–Bloembergen–Morgan theory. The data analysis was performed assuming the orbital angular momentum $L = 0$ for Gd-DOTA and the aqua ion $[Mn(H_2O)_6]^{2+}$ and $L \neq 0$ for Dy-, Tb-, and Er-DOTA. A refined estimation of the zero-field-splitting barrier Δ and of the modulation correlation time τ_v was obtained for $[Mn(H_2O)_6]^{2+}$ by extending the fitting of nuclear magnetic relaxation dispersion profiles to the low-field regime. The Gd-DOTA fitting parameters resulted in good agreement with the literature, and the fit of transverse relaxivity data confirmed the negligibility of the scalar interaction in the nuclear relaxation mechanism. Larger transverse relaxivities of Dy-DOTA and Tb-DOTA ($\sim$10 mM^{-1} s^{-1}) with respect to Er-DOTA ($\sim$1 mM^{-1} s^{-1}) were observed at 16 T. Such higher values are suggested to be due to a shorter residence time τ_m that is possibly linked to the fluctuations of the hyperfine interaction and the different shape of the magnetic anisotropy. The possible employment of Dy-DOTA, Tb-DOTA, and Er-DOTA as negative magnetic resonance imaging contrast agents for high-field applications was envisaged by collecting spin-echo images at 7 T. Particularly in Dy- and Tb-derivatives, the transverse relaxivity at 16 T is of the order of the Gd-one at 1.5 T.

Published under an exclusive license by AIP Publishing. https://doi.org/10.1063/5.0072185

INTRODUCTION

The Magnetic Resonance Imaging (MRI) contrast agents have been extensively studied in the last 40 years, and their use in medicine is widespread, especially for the most common applications at 1.5 and 3 T,[1] The main property that allows these systems to enhance the MRI sensitivity is the ability of improving the image contrast, taking advantage of their capability to increase the nuclear relaxation rates. For their characterization, Nuclear Magnetic Resonance (NMR) is commonly employed for collecting nuclear relaxivity data, i.e., the relaxation rate increment (with respect to the pure solvent) normalized to 1 mM concentration of the contrast agent (CA), as a function of Larmor resonance frequency $v = (\gamma/2\pi)B_0$, where γ is the gyromagnetic ratio of the nuclear species, usually ^1H, and B_0 is the applied static magnetic field. The acquired data generate the so-called Nuclear Magnetic Relaxation Dispersion (NMRD) profiles, which can be analyzed according to models based on Solomon–Bloembergen–Morgan (SBM) theory[2–5] for

obtaining information on the chemical exchange time, the minimum approach distance of the water to the magnetic ion, the molecular dynamics (Brownian rotation), and the electron spin dynamics and the magnetic interactions of the CA molecule with the surrounding environment.[6–8]

The MRI CAs are usually composed of a paramagnetic center, typically a metal ion, surrounded by a chelate, which allows biological compatibility and favors the "safe" residence in the body and the correct elimination from the organism of the CA after its injection.[1] Their design is based on the Paramagnetic Relaxation Enhancement (PRE) mechanism,[9] which causes a local increase in both nuclear longitudinal $R_1 = 1/T_1$ and transverse $R_2 = 1/T_2$ relaxation rates of tissues, where T_1 is the spin–lattice relaxation time and T_2 is the spin–spin relaxation time. The PRE mechanism causes the desired improvement of the image contrast and, depending on their effect on T_1 or T_2, CAs can be classified as follows: (i) *positive* CAs that produce brighter zones reducing mainly T_1 and (ii) *negative* CAs that cause darker spots reducing mainly T_2. For obtaining generally a positive contrast, as a paramagnetic center, the Gd(III) ion provides the best nuclear relaxation rate enhancement, if compared to the other ions of the lanthanide series, due to its long electronic relaxation time. This occurrence explains the extensive employment of Gd(III) complexes as positive CA in MRI. Other Ln(III) complexes [especially Dy(III) complexes], characterized by short electronic relaxation times, are more often used as shift agents for NMR spectroscopic applications. On the other hand, because of the recent development of very high-field scanners for the human body,[10–13] materials belonging to the same family of the most used CAs, but scarcely explored, have been suggested.[14–16] The example of such materials is the non-Gd Ln(III)-based compounds[17–19] that, as their paramagnetic transverse relaxation rate contribution depends on the square of the chemical shift (proportional to the magnetic field),[19,20] have been proposed as potential negative CAs for high-field applications.

In the present work, we investigated the NMRD profiles of four different Ln(III)-DOTA complexes in aqueous solutions (Ln = Gd, Tb, Dy, Er; DOTA = 1,4,7,10-tetraazacyclododecane-N,N′,N″,N‴-tetraacetic acid) and of $[Mn(H_2O)_6]^{2+}$ aqua ions for comparison, combining the analysis of both longitudinal and transverse relaxivity data acquired in a wide range of frequencies (from 10 kHz up to 700 MHz). According to the literature, this combined approach allows us to determine the main physico-chemical quantities that influence the MRI contrast agent's efficiency.[19] The data were analyzed considering both the quenched [Gd(III) and Mn(II)] or unquenched [Dy(III), Tb(III) and Er(III)] orbital angular momentum, and the presence of the so-called Curie relaxation.[21] The latter contribution is efficient when the magnetic dipolar interaction between the nuclear spins and the thermal average of the electronic spin is modulated by the molecular motion. Notably, the Curie contribution is singled out when the electronic correlation time is short.[22,23]

Furthermore, the efficiency of Dy-DOTA, Tb-DOTA, and Er-DOTA at high fields as both positive and negative MRI CAs is shown in contrast images collected at 7 T employing a pre-clinical scanner.

In the sections titled Theory, Experimental Details, Data Analysis and Discussion, and Conclusions, we will present the theoretical basis of models of longitudinal and transverse NMRD profiles,

the experimental details, the obtained results, and the correlated discussion.

THEORY

The relaxation rate enhancements caused by a paramagnetic species diluted in a diamagnetic solvent (e.g., water) can be expressed as

$$R_{i,p} = r_i C = R_{i,obs} - R_{i,dia} \quad \text{with } i = 1, 2, \tag{1}$$

where $R_{i,obs}$ and $R_{i,dia}$ are the relaxation rates of the solution and of the solvent, respectively, while the paramagnetic contribution $R_{i,p}$ is expressed in terms of the concentration of the paramagnetic species C, usually given in mM (1 mM = 1 mmol l^{-1}), and of the relaxivity r_i (in units of mM^{-1} s^{-1}). The paramagnetic terms $R_{i,p}$ can be separated in two sub-terms, according to the intra- or inter-molecular nature of the interactions, namely, the inner-sphere (IS) and outer-sphere (OS) contribution, respectively: $R_{i,p} = R_{i,IS} + R_{i,OS}$.

Let us now split the theoretical model into two cases depending on the characteristics of the paramagnetic center: (i) for Gd-DOTA and $[Mn(H_2O)_6]^{2+}$, $L = 0$ and negligible Curie contribution, and (ii) for Dy(III), Tb(III), and Er(III) complexes, $L \neq 0$ and non-negligible Curie contribution. The motivation of this choice is correlated with the different interactions considered in the SBM model: In the former case, the dipolar and scalar interactions dominate the relaxation mechanism due to long electronic correlations times ($\gg 1$ ps); in the second case, due to short relaxation times (<1 ps), the dipolar and scalar interactions give a much smaller contribution to the nuclear relaxation, and at high fields, the Curie contribution dominates.

Therefore, we considered two ions with $L = 0$, i.e., Gd(III) and Mn(II). Indeed, Gd(III) represents a standard in MRI, and it is widely used. Conversely, Mn(II) has been poorly exploited so far, but it has been recently proposed as a valid alternative to Gd(III) complexes.[24–26]

Among the possible anisotropic lanthanide ions, we have chosen Dy(III), Tb(III), and Er(III) due to several reasons. From a chemical point of view, these ions have similar radii and comparable kinetic constants for the solvent exchange processes.[27–30] The magnetic anisotropy of all these ions is comparable and remarkably high at room temperature. A plot of susceptibility tensors of these ions in the Ln-DOTA complexes, computed at room temperature using crystal field parameters recently reported for the whole DOTA series,[31] is reported in Fig. 1. The magnetic anisotropy of Dy and Tb is substantially easy plane, while the magnetic anisotropy of Er is easy axis.

Case 1: Orbital angular momentum *L* = 0

For ions characterized by null orbital angular momentum ($L = 0$), such as Gd(III) and Mn(II), the two major contributions to the relaxivity arise from the dipolar (DD) and the scalar (also named contact or hyperfine, SC) interactions. The contribution from the Curie can be neglected.[1]

The equations expressing the inner-sphere contribution of the longitudinal and transverse relaxation rates $R_{i,IS}$ are given as follows:

$$R_{1,IS} = \left(\frac{1}{T_1}\right)^{IS} = fq\frac{1}{T_{1m} + \tau_m}, \tag{2}$$
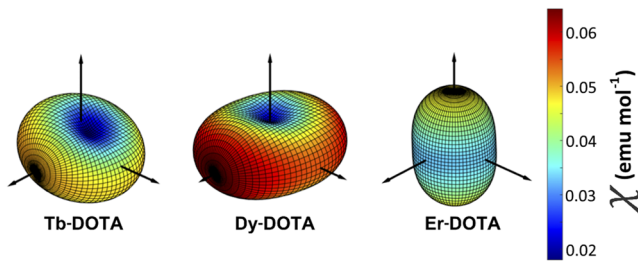
FIG. 1. Magnetic susceptibility tensor of Dy-DOTA, Tb-DOTA, and Er-DOTA calculated at T = 298 K and μ_0H = 1 T using the crystal field parameters reported in the recent work of Briganti *et al.*[31] The color scale refers to the value of the magnetic susceptibility. The vertical arrow in the three plots coincides with the direction of the lanthanide–water bond.

$$R_{2,IS} = \left(\frac{1}{T_2}\right)^{IS} = \frac{fq}{\tau_m}\frac{T_{2m}^{-2} + \tau_m^{-1}T_{2m}^{-1} + \Delta\omega_m^2}{\left(\tau_m^{-1} + T_{2m}^{-1}\right)^2 + \Delta\omega_m^2}, \quad (3)$$

where f is the ratio between the concentration of the paramagnetic species and the water ($f = C/55\,500$), q is the number of bound water molecules per paramagnetic ion (hydration number), T_{im} are the proton relaxation times (with i = 1, 2) of the coordinated water, τ_m is the lifetime of the first coordination sphere's water molecules of the complex exchanging with the bulk (also known as water exchange time), and $\Delta\omega_m$ is the chemical shift of the coordinated water molecule. In particular, $\Delta\omega_m$ is proportional to the magnetic field and results from the sum of a contact term $\Delta\omega_m^{cont} = g\mu_B S(S + 1)(A/\hbar)[1/(3k_B T)]B_0$, where B_0 is the applied magnetic field, k_B is the Boltzmann constant, and T is the temperature, and the one related to the rotational average of the dipole–dipole interaction (also known as the pseudocontact).[1,19,32] The equations for the two different contributions (DD and SC) to the proton relaxation rates ($1/T_{im}$) of the coordinated water molecule are as follows:

$$\left(\frac{1}{T_{im}}\right) = \left(\frac{1}{T_i^{DD}}\right)^{IS} + \left(\frac{1}{T_i^{SC}}\right)^{IS} \quad \text{with } i = 1, 2, \quad (4)$$

$$\left(\frac{1}{T_1^{DD}}\right)^{IS} = \frac{2}{15}\left(\frac{\mu_0}{4\pi}\right)^2\frac{\gamma_I^2 g^2 \mu_B^2}{r^6}S(S + 1)$$
$$\times\left[7\frac{\tau_{c2}}{1 + \omega_S^2\tau_{c2}^2} + 3\frac{\tau_{c1}}{1 + \omega_I^2\tau_{c1}^2}\right], \quad (5)$$

$$\left(\frac{1}{T_1^{SC}}\right)^{IS} = \frac{2S(S + 1)}{3}\left(\frac{A}{\hbar}\right)^2\left(\frac{\tau_{e2}}{1 + \omega_S^2\tau_{e2}^2}\right), \quad (6)$$

$$\left(\frac{1}{T_2^{DD}}\right)^{IS} = \frac{1}{15}\left(\frac{\mu_0}{4\pi}\right)^2\frac{\gamma_I^2 g^2 \mu_B^2}{r^6}S(S + 1)$$
$$\times\left[13\frac{\tau_{c2}}{1 + \omega_S^2\tau_{c2}^2} + 3\frac{\tau_{c1}}{1 + \omega_I^2\tau_{c1}^2} + 4\tau_{c1}\right], \quad (7)$$

$$\left(\frac{1}{T_2^{SC}}\right)^{IS} = \frac{S(S + 1)}{3}\left(\frac{A}{\hbar}\right)^2\left(\frac{\tau_{e2}}{1 + \omega_S^2\tau_{e2}^2} + \tau_{e1}\right), \quad (8)$$

where γ_I is the gyromagnetic ratio of the observed nucleus, g is the electron g-factor, μ_B is the Bohr magneton, r is the distance between the paramagnetic ion and the observed nucleus, S is the spin quantum number, μ_0 is the vacuum magnetic permeability, $A/\hbar$ is the scalar (or hyperfine) coupling constant between the electron spin of the paramagnetic ion and the proton spin of the coordinated water, and ω_I and ω_S are the nuclear and electron angular precession frequencies. The correlation times τ_{ci} and τ_{ei} (i = 1, 2) modulate the dipolar and the scalar interactions and are given by $\tau_{ci}^{-1} = \tau_m^{-1} + \tau_r^{-1} + T_{ie}^{-1}$ and $\tau_{ei}^{-1} = \tau_m^{-1} + T_{ie}^{-1}$, where τ_r is the rotational correlation time of the complex and T_{ie} (i = 1, 2) are the electronic relaxation times. In the Redfield limit[33] (see below) and for metal complexes with $S \geq 1$, the electronic relaxation rates ($1/T_{ie}$) are usually written by taking into account the zero-field-splitting (ZFS) interaction as follows:

$$\left(\frac{1}{T_{1e}}\right)^{ZFS} = 2\tilde{C}\left(\frac{1}{1 + \omega_S^2\tau_v^2} + \frac{4}{1 + 4\omega_S^2\tau_v^2}\right), \quad (9)$$

$$\left(\frac{1}{T_{2e}}\right)^{ZFS} = \tilde{C}\left(\frac{5}{1 + \omega_S^2\tau_v^2} + \frac{2}{1 + 4\omega_S^2\tau_v^2} + 3\right) \quad (10)$$

with $\tilde{C} = 1/50\,\Delta^2\tau_v[4S(S + 1) - 3]$, where Δ^2 is the mean squared fluctuation of the ZFS,[57] which is related to the ZFS parameters D_{ZFS} and E_{ZFS} (i.e., the axial and transverse component of the magnetic anisotropy) by the relation $\Delta = \sqrt{2/3D_{ZFS}^2 + 2E_{ZFS}^2}$, and τ_v is the ZFS modulation correlation time. $\tilde{C}$ can be expressed in terms of the low-field electronic relaxation time τ_{S0} as $\tilde{C} = 0.1/\tau_{S0}$ in order to highlight its temporal meaning. In the limit $\omega_S^2\tau_v^2 \ll 1$, $T_{1e} = T_{2e} = \tau_{S0}$. The Redfield limit is given by $\Delta^2\tau_v^2 \ll 1$.

The equations for the outer-sphere longitudinal and transverse proton relaxation rates of bulk water molecules $R_{i,OS} = (1/T_i^{DD})^{OS}$ (with i = 1, 2) are related only to the dipolar interaction and are given as follows:

$$\left(\frac{1}{T_1^{DD}}\right)^{OS} = \frac{32\pi}{405}\left(\frac{\mu_0}{4\pi}\right)^2\frac{N_A C}{dD}\gamma_I^2 g^2 \mu_B^2 S(S + 1)$$
$$\times[7j_2(\omega_S) + 3j_1(\omega_I)], \quad (11)$$

$$\left(\frac{1}{T_2^{DD}}\right)^{OS} = \frac{16\pi}{405}\left(\frac{\mu_0}{4\pi}\right)^2\frac{N_A C}{dD}\gamma_I^2 g^2 \mu_B^2 S(S + 1)$$
$$\times[13j_2(\omega_S) + 3j_1(\omega_I) + 4j_1(0)], \quad (12)$$

where N_A is the Avogadro number, d is the distance of minimum approach for bulk water molecules to the paramagnetic center, D is the relative self-diffusion constant, and $j_k(\omega)$ is the spectral density function for the dipolar interaction given by

$$j_k(\omega) = \text{Re}\left\{\frac{1 + z/4}{1 + z + 4z^2/9 + z^3/9}\right\}, \quad (13)$$

where $z = \sqrt{i\omega\tau_D + \tau_D/T_{ke}}$ (with k = 1, 2) and $\tau_D = d^2/D$ is the translational correlation time.

Case 2: Orbital angular momentum $L \neq 0$

For ions characterized by non-null orbital angular momentum ($L \neq 0$), such as Dy(III), Tb(III), and Er(III), the electronic relaxation time is shorter, the DD and SC contributions are small, and as a consequence, the Curie contribution dominates at high fields.[19,22]

The equations for the inner-sphere contributions of the longitudinal and transverse relaxation rates $R_{i,IS}$ are again given by Eqs. (1) and (2), but the proton relaxation rates are now expressed as follows:

$$\left(\frac{1}{T_{im}}\right) = \left(\frac{1}{T_i^{DD}}\right)^{IS} + \left(\frac{1}{T_i^{SC}}\right)^{IS} + \left(\frac{1}{T_i^{Curie}}\right)^{IS} \quad \text{with } i = 1, 2. \quad (14)$$

The equations for the inner-sphere terms [Eqs. (5)–(8)] are still valid when applying the following corrections: g must be substituted with the Landé g-factor g_j, and S must be substituted with the total spin quantum number J. The Curie contributions to the proton relaxation rates are expressed as

$$\left(\frac{1}{T_1^{Curie}}\right)^{IS} = \frac{2}{5}\left(\frac{\mu_0}{4\pi}\right)^2 \frac{\gamma_I^2 B_0^2 g_j^4 \mu_B^4 J^2 (J+1)^2}{r^6} \frac{1}{(3k_B T)^2}$$
$$\times \left[\frac{3\tau_{cc}}{1 + \omega_S^2 \tau_{cc}^2}\right], \quad (15)$$

$$\left(\frac{1}{T_2^{Curie}}\right)^{IS} = \frac{1}{5}\left(\frac{\mu_0}{4\pi}\right)^2 \frac{\gamma_I^2 B_0^2 g_j^4 \mu_B^4 J^2 (J+1)^2}{r^6} \frac{1}{(3k_B T)^2}$$
$$\times \left[\frac{3\tau_{cc}}{1 + \omega_I^2 \tau_{cc}^2} + 4\tau_{cc}\right]. \quad (16)$$

The equations for the outer-sphere contributions result now from the sum of two terms, the dipolar and the Curie ones, and assume the form

$$R_{i,OS} = \left(\frac{1}{T_i^{DD}}\right)^{OS} + \left(\frac{1}{T_i^{Curie}}\right)^{OS} \quad \text{with } i = 1, 2, \quad (17)$$

$$\left(\frac{1}{T_1^{DD}}\right)^{OS} = \frac{16\pi}{135}\left(\frac{\mu_0}{4\pi}\right)^2 \frac{N_A C}{dD} \gamma_I^2 g^2 \mu_B^2$$
$$\times \left\{ 6 \left[J(J+1) - S_c \coth\frac{\chi}{2J} - S_c^2 \right] j_1(\omega_I) \right.$$
$$\left. + 7 \coth\frac{\chi}{2J} S_c j_2(\omega_S) \right\}, \quad (18)$$

$$\left(\frac{1}{T_2^{DD}}\right)^{OS} = \frac{16\pi}{135}\left(\frac{\mu_0}{4\pi}\right)^2 \frac{N_A C}{dD} \gamma_I^2 g^2 \mu_B^2$$
$$\times \left\{ \left[J(J+1) - S_c \coth\frac{\chi}{2J} - S_c^2 \right] \right.$$
$$\left. \times (3j_1(\omega_I) + 4j_1(0)) \right\}$$
$$+ \frac{16\pi}{135}\left(\frac{\mu_0}{4\pi}\right)^2 \frac{N_A C}{dD} \gamma_I^2 g^2 \mu_B^2$$
$$\times \left[6.5 \coth\frac{\chi}{2J} S_c j_2(\omega_S) \right], \quad (19)$$

$$\left(\frac{1}{T_1^{Curie}}\right)^{OS} = \frac{32\pi}{45}\left(\frac{\mu_0}{4\pi}\right)^2 \frac{N_A C}{dD} \gamma_I^2 g^2 \mu_B^2 S_c^2 j(\omega_I), \quad (20)$$

$$\left(\frac{1}{T_2^{Curie}}\right)^{OS} = \frac{16\pi}{45}\left(\frac{\mu_0}{4\pi}\right)^2 \frac{N_A C}{dD} \gamma_I^2 g^2 \mu_B^2 S_c^2 \{3j(\omega_I) + 4j(0)\}, \quad (21)$$

where $\chi = J B_0 \mu_B g_j /(k_B T)$ and $S_c = J B_J(\chi)$ is the time-averaged or "Curie" spin given by the product of J with the Brillouin function $B_J(\chi)$,[21,34] τ_{cc} is the correlation time for the Curie contribution ($\tau_{cc}^{-1} = \tau_m^{-1} + \tau_r^{-1}$), and $j(\omega)$ is the spectral density function for the dipolar interaction $j_k(\omega)$ in the limit of $T_{ie} \to \infty$.

EXPERIMENTAL DETAILS

Sample preparation

Crystalline powders of Na[LnDOTA(H$_2$O)]·4H$_2$O with Ln(III) = Gd(III), Dy(III), Tb(III), and Er(III) and DOTA = 1,4,7,10-tetraazacyclododecane-N,N',N'',N'''-tetraacetic acid were obtained following the procedure reported in previous works.[35–37]

Manganese(II) chloride tetrahydrate powders (formula MnCl$_2$·4H$_2$O, molar mass 197.91 g/mol) were supplied by Sigma-Aldrich Co., St. Louis, MO, USA.

All the solutions were prepared by diluting the compound powders in MilliQ water and obtaining the following concentrations: [MnCl$_2$] = 0.65 mM, [Gd-DOTA] = 1.082 mM, [Dy-DOTA] = 17.3 mM, [Tb-DOTA] = 11 mM, and [Er-DOTA] = 15.5 mM. The evaluation of the chemical shifts for the LnDOTA complexes (Ln ≠ Gd) was performed by collecting the solution spectra at 400 and 700 MHz and by adding a small amount of trimethylsilylpropanoic acid (TSP) sodium salt as internal reference: this step was done after the acquisition of all the NMRD profiles. Furthermore, two additional sets of Dy-DOTA, Tb-DOTA, and Er-DOTA samples with 100 and 5 mM concentrations were prepared for low-field T_2 measurements ($\nu \leq 3$ MHz) and MRI acquisitions, respectively.

NMR relaxometry

The NMRD profiles of the different aqueous solutions were acquired at room temperature $T = 298$ K by measuring the spin–lattice relaxation time T_1 and the spin–spin relaxation time T_2 at several Larmor resonance frequencies (i.e., at different external magnetic field strengths). Several devices and techniques, summarized in Table I, were employed to span a wide range of frequencies ν, from 0.01 MHz up to 700 MHz, corresponding to a broad range of magnetic field strength $2.35 \times 10^{-4} < \mu_0 H < 16$ T.

We employed standard NMR techniques[38] for relaxation time measurements above 7.2 MHz, while below 7.2 MHz, we used the Fast-Field-Cycling (FFC) techniques.[39,40] All T_1 measurements were performed by employing either the saturation or the inversion recovery pulse-sequences. To quantify T_2, we used the Carr–Purcell–Meiboom–Gill (CPMG) sequence for frequency above 3 MHz and the Spin-Echo (SE) sequence for frequency below 3 MHz. The raw data were then fitted with an exponential recovery function for T_1 (signal intensity vs different saturation/inversion times) or with an exponential decay function for T_2 (signal intensity vs different echo-times). An experimental error of 8% was assigned

TABLE I. NMRD profile acquisition instrumentation and techniques according to specific ranges of frequencies. As from the main text, hereafter are reported the meanings of the acronyms used in the table: FFC = Fast Field Cycling, PP = Pre-Polarized, NP = Non-Polarized, CPMG = Carr–Purcell–Meiboom–Gill, and NMR = Nuclear Magnetic Resonance.

Frequency (MHz)	Instrumentation	Techniques
0.01–3	Stelar[a] SMARTracer relaxometer	FFC-PP (saturation recovery + spin echo)
3–7.2	Stelar[a] SMARTracer relaxometer	FFC-NP (saturation recovery + CPMG)
7.2–60	Stelar[a] Spinmaster spectrometer	NMR (saturation recovery + CPMG)
7.2–298	Tecmag[b] Apollo spectrometer + Bruker[c] electromagnet/superconducting magnet	NMR (saturation recovery + CPMG)
400	Bruker[c] FT-NMR Avance spectrometer	NMR (inversion recovery + CPMG)
700	Bruker[c] Avance NEO spectrometer	NMR (inversion recovery + CPMG)

[a]Stelar s.r.l., Mede, Italy.
[b]Tecmag, Houston, TX, USA.
[c]Bruker Corporation, Billerica, MA, USA.

to all the experimental data based on previous studies on the systematic error outlined for the different experimental setups due to the electronic chain.

In vitro magnetic resonance imaging

MRI acquisitions were performed at 0.18 T ($v = 7.74$ MHz) on an Artoscan Imager (Esaote, Genova, Italy) and at 7 T ($v = 298$ MHz) on a PharmaScan scanner (Bruker, Billerica, MA, USA). The images of 2 ml vials filled with 5 mM aqueous solutions of Dy-DOTA, Tb-DOTA, and Er-DOTA were acquired at room temperature. We acquired two series of spin-echo images for each magnetic field strength: the first one varying the repetition time (TR) and the second one changing the echo time (TE). The acquisition parameters can be summarized as follows:

- *Esaote Artoscan Imager* (0.18 T, $v = 7.74$ MHz):
  1. T_1-weighted sequence. TR = 100, 300, 500 ms, TE = 20 ms, acquisition matrix 256 × 192, reconstruction matrix 256 × 256, FOV = 12 × 12 cm^2, slice thickness = 5 mm, and average = 10.
  2. T_2-weighted sequence. TE = 28, 90, 120 ms, TR = 2.8 s, acquisition matrix 256 × 192, reconstruction matrix 256 × 256, FOV = 12 × 12 cm^2, slice thickness = 5 mm, and average = 1.
- *Bruker PharmaScan scanner* (7 T, $v = 298.03$ MHz):
  1. T_1-weighted sequence. TR = 100, 300, 500 ms, TE = 20 ms, acquisition matrix 256 × 192, reconstruction matrix 256 × 256, FOV = 4 × 4 cm^2, slice thickness = 1 mm, and average = 3.
  2. T_2-weighted sequence. TE = 28, 90, 120 ms, TR = 2.8 s, acquisition matrix 256 × 192, reconstruction matrix 256 × 256, FOV = 4 × 4 cm^2, slice thickness = 1 mm, and average = 1.

DATA ANALYSIS AND DISCUSSION

The NMRD profiles were fitted with the model functions described in the section titled Theory using a custom Matlab script (MathWorks, Natick, MA, USA). The proton longitudinal and

transverse relaxivity experimental data and the fitting curves of the five samples are reported in Fig. 2 (case 1, Gd-DOTA and [Mn(H$_2$O)$_6$]$^{2+}$) and Fig. 3 (case 2, Dy-DOTA, Tb-DOTA, and Er-DOTA). The parameters of each fit are reported in Table II (case 1) and Table III (case 2).

The obtained results are separately discussed below.

Case 1: [Mn(H$_2$O)$_6$]$^{2+}$

Experimental data for [Mn(H$_2$O)$_6$]$^{2+}$, Fig. 2, were fitted with Eq. (1) using the expressions reported in Eqs. (2)–(13) and the parameters in Table II(a). In Table II(a), we also indicate fixed and adjustable parameters employed for the least-squares fitting procedure. The different contributions to the relaxivities described in the section titled Theory are shown in Fig. S1(a) of the supplementary material.

From the fitting of r_1 data, we estimated r, τ_r, $A/\hbar$, τ_{S0}, and τ_v. The obtained values were thus fixed for the analysis of r_2, from which the values of τ_m and of the ZFS parameter τ_v were extracted. For the sake of clarity, it should be noted that the fit of r_1 resulted insensitive to values of $\tau_m > 1$ ns since the conditions $T_{1m} \gg \tau_m$ and $\tau_r \ll \tau_m$ hold. As τ_v and τ_{S0} were thus estimated, it was possible to calculate the mean squared fluctuations of the ZFS parameter Δ^2. It is worth remarking that the estimation of τ_v obtained from the fitting of r_1 data suffers from a great uncertainty, in analogy with the results of the work of Gomez *et al.* in 2014.[41] Indeed, ZFS parameters can be hardly retrieved by NMR acquisitions only,[42,43] mainly if limited to the longitudinal relaxivity NMRD profile alone.[1]

The increase in the transverse relaxivity at frequency $v > 20$ MHz is principally due to the SC contribution, which is a non-negligible mechanism different from the situation of the other DOTA complexes here investigated. The pseudocontact contribution to $\Delta\omega_m$ was neglected.

It is important to remark that by extending the data acquisition to the low frequency regime and combining the analysis of r_1 and r_2 NMRD profiles, we were able to directly obtain an estimation of τ_m, which is usually determined through ^{17}O NMRD profile analysis,[41–44] and a more accurate evaluation of τ_v and Δ^2.[24,41,45,46]
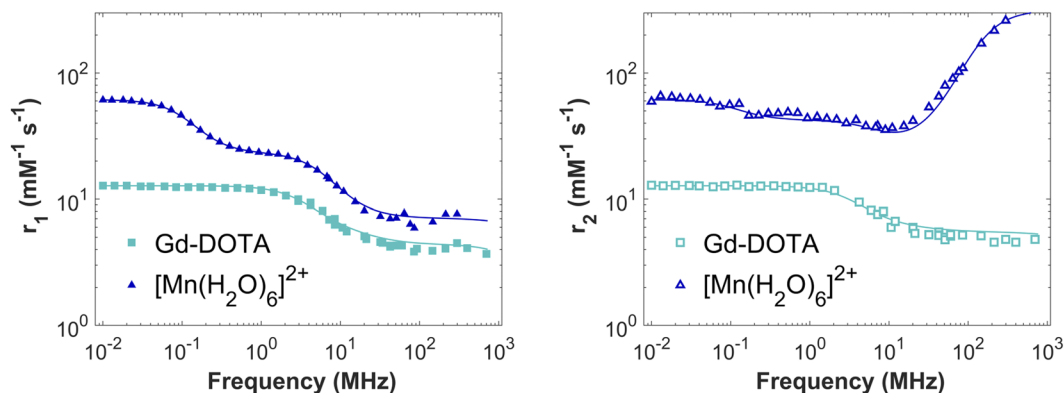
FIG. 2. Longitudinal (left) and transverse (right) relaxivitiy ^1H NMRD profiles of Gd-DOTA and $[Mn(H_2O)_6]^{2+}$ solutions at 298 K. The lines represent the best fit curves using the Solomon–Bloembergen–Morgan equations (see the text).
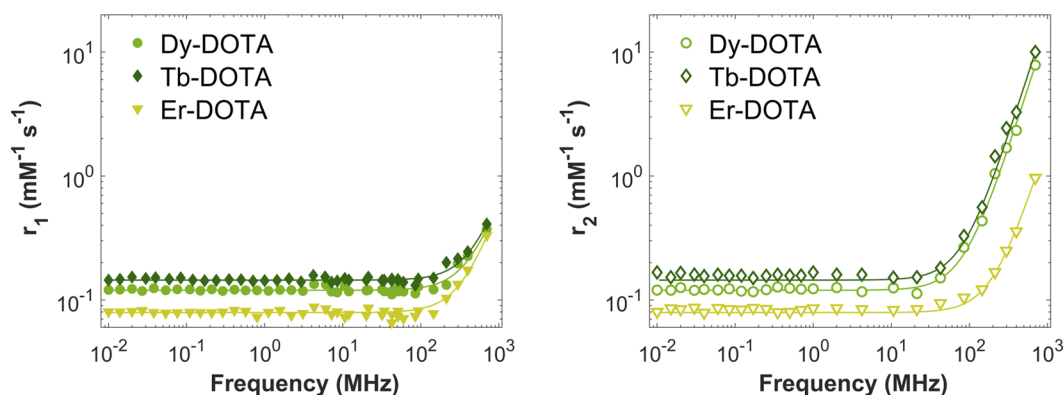

FIG. 3. Longitudinal (left) and transverse (right) relaxivitiy ^1H NMRD profiles of Dy-DOTA, Tb-DOTA, and Er-DOTA solutions at 298 K. The lines represent the best fit curves using the Solomon–Bloembergen–Morgan equations (see the text).

TABLE II. Parameters obtained from the fitting of (a) $[Mn(H_2O)_6]^{2+}$ and (b) Gd-DOTA solution NMRD profiles. Underscored parameters are those kept fixed in the least-squares fitting procedure. The values in parentheses represent the standard deviation of the fitted parameter. The fixed parameter values for the r_2 data analysis and obtained from the r_1 data fitting are labeled with the apical asterisk. The values of the parameters reported in italics were calculated through the relation $\tau_{S0}^{-1} = 1/5\{4S(S+1) - 3\}\Delta^2;\tau_V$ their standard deviations, if any, were obtained by the propagation of uncertainties.

Parameter	(a) $[Mn(H_2O)_6]^{2+}$			(b) Gd-DOTA		
	r_1	r_2	References 41/45/47/46	r_1	r_2	Reference 42
q	6	6	6/6/6	1	1	1
r (Å)	2.89 (0.04)	2.89*	2.83/2.78/2.71 (0.03)	3.07 (0.05)	3.05 (0.07)	3.1
τ_r (ps)	38.6 (2.9)	38.6*	30.0 (0.2)/32/32 (2)	78.1 (8.5)	81.5 (12.8)	77 (4)
τ_m (ns)	35.5	37.3 (0.7)	35.5 (4.0)/···/20	244	244	244 (11)
$A/\hbar$ (Mrad s^{-1})	5.37 (0.08)	5.37*	5.43 (0.03)/4.27/5.1 (0.5)	···	···	···
τ_{S0} (ps)	2267 (42)	2267*	···/3500/3500	486.7 (47.8)	445.8 (58.2)	473 (52)
τ_v (ps)	0.5 (0.5)	4.34 (0.10)	10 (10)/2–3/5.3	11	11	11 (1)
$\Delta^2/10^{19}$ (s^{-2})	···	1.59 (0.05)	0.06 (0.06)/1.5–2.2/0.84	1.56 (0.16)	1.70 (0.26)	1.6 (0.1)
d (Å)	3.6	3.6	3.6/···/···	3.5	3.5	3.5
$D/10^{-9}$ ($m^2\ s^{-1}$)	2.3	2.3	2.3/···/···	2.3	2.3	2.2

TABLE III. Parameters obtained from the fitting of Dy-DOTA, Tb-DOTA, and Er-DOTA solution NMRD profiles and from the analysis of the 400 and 700 MHz NMR ^{1}H spectra as explained in the text. Underscored parameters are those kept fixed in the least-squares fitting procedure. The values in parentheses represent the standard deviation of the fitted parameter. The values fixed for the r_2 data analysis and obtained from the r_1 data fitting procedures are labeled with the apical asterisk.

Parameter	Dy-DOTA		Tb-DOTA		Er-DOTA	
	r_1	r_2	r_1	r_2	r_1	r_2
r (Å)	3.37 (0.05)	3.37*	2.96 (0.05)	2.96*	3.02 (0.05)	3.02*
τ_{S0} (ps)	0.19 (0.01)	0.19*	0.22 (0.01)	0.22*	0.13 (0.01)	0.13*
α (Mrad s^{-1} T^{-1})	$\cdots$	0.31 (0.01)	$\cdots$	0.27 (0.01)	$\cdots$	0.21 (0.01)
τ_m (ns)	<u>10</u>	15.39 (0.05)	<u>10</u>	26.39 (0.07)	<u>10</u>	1.40 (0.03)
τ_m (ns) (spectra)	$\cdots$	16.91 (1.15)	$\cdots$	29.36 (2.20)	$\cdots$	4.84 (0.34)

As reported in Table II(a), a good agreement of all the estimated parameters with the literature ones was found (r = 2.89 ± 0.04 Å, τ_r = 38.6 ± 2.9 ps, and τ_{S0} = 2267 ± 42 ps).[41,45–47]

Case 1: Gd-DOTA

The data of Gd-DOTA, Fig. 2, were fitted with Eq. (1) using the expressions reported in Eqs. (2)–(13) and the parameters in Table II(b) (even in this case, fixed and adjustable parameters are highlighted). The contributions to the relaxivities described in the section titled Theory are reported in Fig. S1(b) of the supplementary material.

As in previous studies,[42,48] the scalar contributions [Eqs. (4) and (6)] to the relaxivities were neglected in the present case. Indeed, the dispersions of relaxivity data due to the scalar term and the related high-field increase in r_2 are absent [see [Mn(H$_2$O)$_6$]$^{2+}$ data for comparison, Fig. S1(a)].

For the fitting of r_1 data, we employed r, τ_r, τ_{S0}, and τ_v as adjustable parameters. Analogously to [Mn(H$_2$O)$_6$]$^{2+}$, the estimation of τ_v from the fitting of the longitudinal NMRD profile was affected by a considerable uncertainty (~100%). Therefore, we decided to fix τ_v to the literature value τ_v = 11 ps.[42]

For r_2 fitting, as the scalar contribution can be neglected ($A/\hbar$ must be lower than 0.1 Mrad/s for a correct fitting of both r_1 and r_2 data), Eq. (3) reduces to $(1/T_2)^{IS}$ = $fq/(T_{2m} + \tau_m)$. This relation has the same form of Eq. (2) since the chemical shift $\Delta\omega_m$ induced on water protons for Gd(III) complexes is due to a pure contact contribution.[19] No further information could therefore be extracted from r_2 data because of the insensitivity to τ_m when the conditions $T_{2m} \gg \tau_m$ and $\tau_r \ll \tau_m$ hold. In this way, we set as adjustable parameters the same ones used for r_1 fitting, i.e., r, τ_r, τ_{S0}, and τ_v. Again, we found a significant uncertainty in estimating the value of τ_v that was therefore fixed to the literature value as done for the r_1 fitting.

Nevertheless, from both the analysis of longitudinal and transverse relaxivity NMRD profiles, we obtained values in good agreement with the literature.[42,48]

Case 2: Dy-DOTA, Tb-DOTA, and Er-DOTA

The data obtained for Dy-, Tb-, and Er-DOTA complexes, Fig. 3, were fitted with Eq. (1) using the expressions reported in Eqs. (2)–(8), where g is substituted by g_J and S is substituted by J, and Eqs. (14)–(21). The contributions to the relaxivities described in the

section titled Theory are highlighted in Fig. S2 of the supplementary material.

We fixed τ_r = 80 ps,[49] d = 3.5 Å (the same value adopted for Gd-DOTA), and D = 2.3 × 10^9 m^2/s,[19] and we hypothesized the electronic relaxation times independent of the applied magnetic field; hence, τ_{S0} = T_{1e} = T_{2e}.[19,22] Moreover, we estimated the ratio between $\Delta\omega_m$ and the applied magnetic field ($\alpha = \Delta\omega_m/B_0$) from the spectra acquired at 400 and 700 MHz (Fig. S3). Extrapolation of $\Delta\omega_m$ was accomplished by measuring the paramagnetic chemical shift $\Delta\omega_p$, which is the shift of the water signal from the diamagnetic position, given by

$$\Delta\omega_p = fq \frac{\Delta\omega_m}{\left(1 + \frac{\tau_m}{T_{2m}}\right)^2 + \tau_m^2 \Delta\omega_m^2}. \tag{22}$$

Equation (22) reduces to $\Delta\omega_p = fq\Delta\omega_m$ if $\tau_m^2 \Delta\omega_m^2 \ll 1$ and $\tau_m/T_{2m} \ll 1$, i.e., when $(T_2^{-1})^{IS}$ is proportional to the square of the magnetic field (at high fields).[20] This behavior can be well appreciated in Fig. 3 (right) for each sample at frequency ν > 20 MHz.

For the three different samples, we obtained r and τ_{S0} from r_1 data fitting, while we extracted the parameter τ_m from the analysis of r_2 data (see Table III).

Observing Fig. 3, some considerations can follow. Er-DOTA showed systematically lower relaxivity values than Dy-DOTA and Tb-DOTA, the last one having the highest relaxivity values, over the whole measured range of frequencies. The differences between the three complexes are evidenced in the high-field region of r_2 data. Indeed, since the three complexes have the same geometrical structure and similar τ_{S0}, τ_v, and α, such differences are mainly attributed to the different water-exchange time τ_m [an independent estimation of τ_m was performed using Eq. (3) combined with the expression for $\Delta\omega_p$ in the limits of $\tau_m^2 \Delta\omega_m^2 \ll 1$ and $\tau_m/T_{2m} \ll 1$, neglecting the OS terms].[20] More in detail, for Er-DOTA, we found τ_m = 1.40 ± 0.03 ns, i.e., one order of magnitude lower than those of Dy-DOTA and Tb-DOTA, for which τ_m = 15.39 ± 0.05 ns (slightly higher than those previously published τ_m = 9 ns)[20] and τ_m = 26.39 ± 0.07 ns, respectively (see Table III). Now, it should be reminded that the electronic distribution of the 4f electrons is different for the three lanthanide ions, being oblate for Dy(III) and Tb(III) and prolate for Er(III).[50] Thus, a possible explanation for the lower value of τ_m of Er-DOTA could be found in the different magnetic anisotropies of these complexes due to their different electronic distributions.[51] In fact, Dy-DOTA and Tb-DOTA complexes are characterized by an

easy-plane magnetic anisotropy, i.e., perpendicular to the Ln-O_w bond (O_w is the oxygen of the coordinated water molecule, which resides at the top of the oxygen plane of the capped square antiprism structure of Ln-DOTA). On the other hand, Er-DOTA is characterized by an easy-axis magnetic anisotropy almost parallel to the Ln-O_w bond, as illustrated in Fig. 1 in the section titled Theory.[35,52–54]

The values obtained for the distances between the lanthanide paramagnetic center and the coordinated water proton are lower than those recently estimated for solid-state Ln-DOTA complexes ($r = 3.4$ Å)[31] but comparable to the geometrical distance assumed for similar complexes (e.g., for Dy-DTPA, Vander Elst et al.[19] assumed $r = 3.1$ Å).

Considering Dy-DOTA, we found $\tau_{S0} = 0.19 \pm 0.01$ ps from measurements at 298 K, which is smaller than the value reported in the literature for the Dy(III) aqua ion at 298 K ($\tau_{S0} = 0.39$ ps)[22] and for Dy-DOTA water solutions at 310 K ($\tau_{S0} = 0.33$ ps).[55,56] Similarly, we found $\tau_{S0} = 0.13 \pm 0.01$ ps (at 298 K) for Er-DOTA that is smaller than the value reported in the literature for the Er(III) aqua ion at 298 K ($\tau_{S0} = 0.31$ ps).[22] No literature data for τ_{S0} were found for Tb-DOTA. As can be seen in detail in Fig. S2, the Curie interaction (dashed lines) is the main responsible for the high-field increase in longitudinal relaxivities observed experimentally, which cannot be described in terms of the dipolar interaction alone (dotted lines).

MRI images

The images of the water solution sample of Dy-DOTA, Tb-DOTA, and Er-DOTA with the same concentration (5 mM) acquired at 0.18 T are reported in Fig. 4 (left), while Fig. 5 (left) shows the MRI acquisitions at 7 T.

Circular ROIs (Regions of Interest) were used to measure the variation of the signal intensity of the vials represented in the images along each series: The graphs on the right in Figs. 4 and 5 illustrate the evolution of the normalized signal intensity as a function of acquisition parameters TR and TE. We found that Tb-DOTA shows the highest enhancement of the relaxation rate, in good agreement with the NMR relaxivity curves [see the top curves on the right side of the graphs reported in Figs. 4(a) and 5(a) and the bottom curves in Figs. 4(b) and 5(b)]. On the counter hand, Er-DOTA displays the lowest enhancement, as shown in Figs. 4(a) and 5(a) (bottom curves in the right side of the graphs) and in Figs. 4(b) and 5(b) (top curves).

It can be also appreciated the contrast enhancement, according to the NMRD profiles, for all three complexes at high fields (7 T, Fig. 5) if compared to low field acquisitions (0.18 T, Fig. 4), especially for the series with variable TE, when comparing the relative increment (varying TR) or decrement (varying TE) of the signal. The TR/TE variations at both fields being equal, the discrepancies between the relative signal intensities are wider along the series at 7 Tesla with respect to those at 0.18 T, indicating shorter relaxation times and, therefore, higher relaxivities.

Thanks to the high-field increment of the transverse relaxivities, Dy-DOTA, Tb-DOTA, and, to a lesser extent, Er-DOTA could be employed as negative MRI contrast agents at high fields. On the other hand, their longitudinal relaxivities are too low for applications as positive contrast agents, despite the high-field growth caused by the Curie interaction.
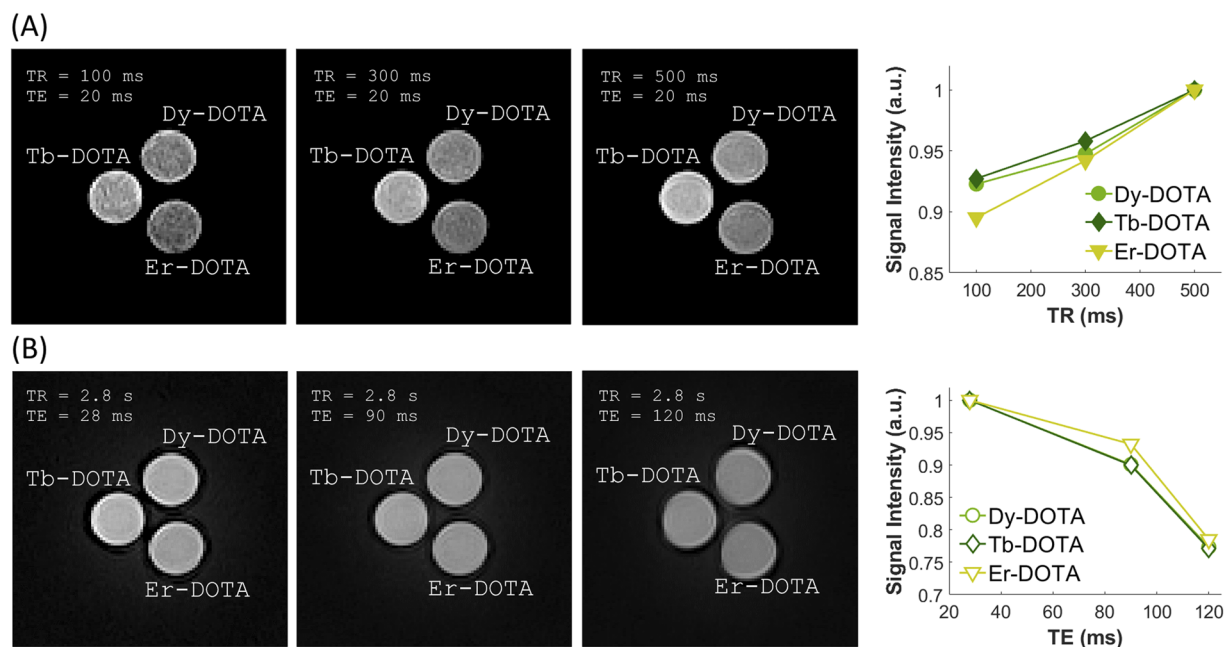

FIG. 4. Low-field MRI acquisitions (0.18 T). Spin-echo images of vials containing 5 mM of Dy-DOTA, Tb-DOTA, and Er-DOTA (a) at different repetition times (TR = 100, 300, 500 ms, TE = 20 ms, acquisition matrix 256 × 192, reconstruction matrix 256 × 256, FOV = 12 × 12 cm^2, slice thickness = 5 mm, and average = 10) and (b) at different echo times (TE = 28, 90, 120 ms, TR = 2.8 s, acquisition matrix 256 × 192, reconstruction matrix 256 × 256, FOV = 12 × 12 cm^2, and slice thickness = 5 mm, and average = 1). The graphs nearby the images show the evolution of the normalized signal intensity measured in circular ROIs for each sample along each series.
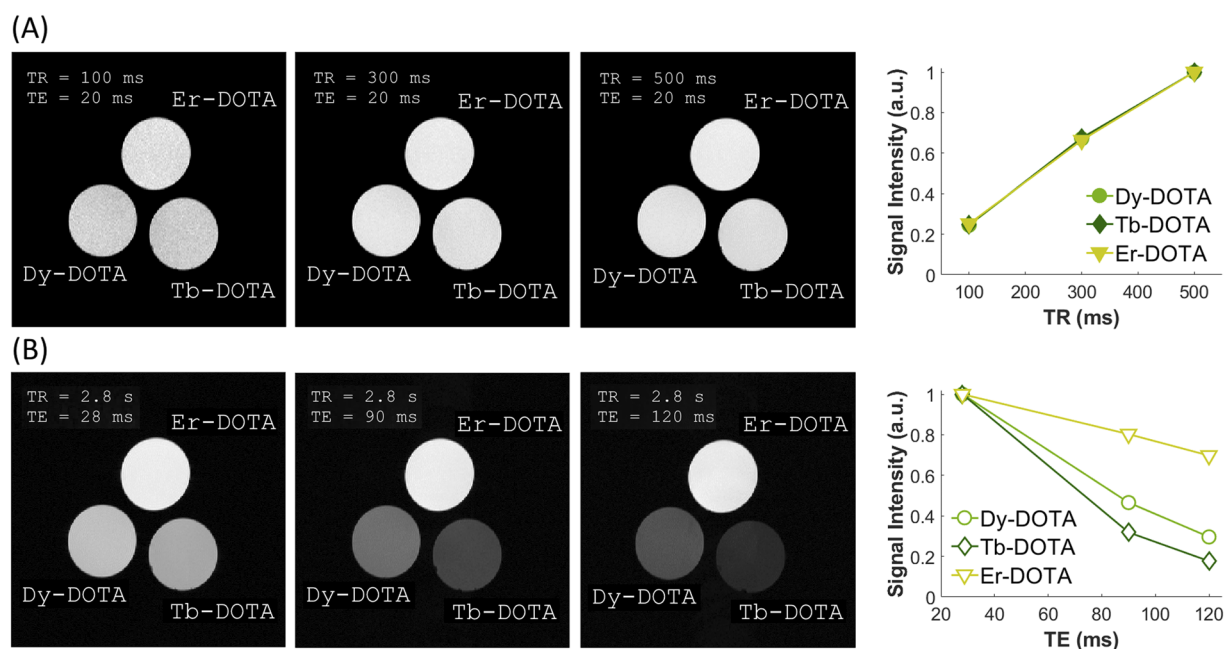
FIG. 5. High-field MRI acquisitions (7 T). Spin-echo images of vials containing 5 mM of Dy-DOTA, Tb-DOTA, and Er-DOTA (a) at different repetition times (TR = 100, 300, 500 ms, TE = 20 ms, acquisition matrix 256 × 192, reconstruction matrix 256 × 256, FOV = 4 × 4 cm^2, slice thickness = 1 mm, and average = 3) and (b) at different echo times (TE = 28, 90, 120 ms, TR = 2.8 s, acquisition matrix 256 × 192, reconstruction matrix 256 × 256, FOV = 4 × 4 cm^2, slice thickness = 1 mm, and average = 1). The graphs nearby the images show the evolution of the normalized signal intensity measured in circular ROIs for each sample along each series.

Further investigations are needed to assess potential pitfalls in terms of biocompatibility and side-effects of these Ln-based complexes for *in vivo* applications.

CONCLUSIONS

The present work provides further evidence of the benefits that could be derived from a combined analysis, not usually performed, of both longitudinal and transverse relaxivity NMRD profiles collected in a wide range of frequencies for the structural, dynamic, and magnetic characterization of MRI contrast agents. For the $[Mn(H_2O)_6]^{2+}$ aqua ion, we were able to assess the water exchange time τ_m directly from the analysis of the NMRD profiles and to give a more accurate estimation of the ZFS parameters, namely, τ_v and Δ^2. It must be mentioned that such a result was obtained without employing other techniques but NMR. Conversely, the fit of the r_2 profile of the Gd-DOTA sample did not provide any additional information if compared to r_1 fitting, but it confirmed (i) the suitability of the SBM model in a wide range of frequencies also for the transverse relaxivity NMRD profiles, often not measured, and (ii) the negligibility of the scalar interaction for the Gd(III) complex. In addition, the analysis of Dy-DOTA, Tb-DOTA, and Er-DOTA NMRD profiles allowed the estimation of the metal–proton distance r, the electronic relaxation times τ_{S0}, and the water exchange times τ_m. We hypothesize that the latter might be correlated with the different magnetic anisotropy of the complexes, easy-plane for Dy-DOTA and Tb-DOTA, and easy-axis for Er-DOTA. Finally, the

possible high-field application as negative MRI CAs for Dy-DOTA, Tb-DOTA, and Er-DOTA complexes was supported by spin-echo images acquired at 7 T. This result could be useful for future high-field clinical imagers and for currently available preclinical MRI scanners.

SUPPLEMENTARY MATERIAL

See the supplementary material to visualize the contributions discussed in the section titled Theory to the NMRD profiles and the NMR spectra acquired at 400 and 700 MHz.

AUTHOR DECLARATIONS

Conflict of Interest

The authors have no conflicts to disclose.

DATA AVAILABILITY

The data that support the findings of this study are available from the corresponding author upon reasonable request.

REFERENCES

[1] A. Merbach, L. Helm, and É. Tóth, *The Chemistry of Contrast Agents in Medical Magnetic Resonance Imaging*, 2nd ed. (John Wiley & Sons, Ltd., 2013).

[2] I. Solomon, "Relaxation processes in a system of two spins," Phys. Rev. **99**, 559–565 (1955).

[3] N. Bloembergen, "Proton relaxation times in paramagnetic solutions," J. Chem. Phys. **27**, 572–573 (1957).

[4] N. Bloembergen and L. O. Morgan, "Proton relaxation times in paramagnetic solutions. Effects of electron spin relaxation," J. Chem. Phys. **34**, 842–850 (1961).

[5] N. Bloembergen, E. M. Purcell, and R. V. Pound, "Relaxation effects in nuclear magnetic resonance absorption," Phys. Rev. **73**, 679–712 (1948).

[6] P. H. Fries and E. Belorizky, "Electronic relaxation of paramagnetic metal ions and NMR relaxivity in solution: Critical analysis of various approaches and application to a Gd(III)-based contrast agent," J. Chem. Phys. **123**, 124510 (2005).

[7] D. Kruk, J. Kowalewski, D. S. Tipikin, J. H. Freed, M. Mościcki, A. Mielczarek, and M. Port, "Joint analysis of ESR lineshapes and ^{1}H NMRD profiles of DOTA-Gd derivatives by means of the slow motion theory," J. Chem. Phys. **134**, 024508 (2011).

[8] K. Ivanov, A. Yurkovskaya, and H.-M. Vieth, "High resolution NMR study of T_1 magnetic relaxation dispersion. I. Theoretical considerations of relaxation of scalar coupled spins at arbitrary magnetic field," J. Chem. Phys. **129**, 234513 (2008).

[9] J. Kowalewski, D. Kruk, and G. Parigi, "NMR relaxation in solution of paramagnetic complexes: Recent theoretical progress for S ≥ 1," Adv. Inorg. Chem. **57**, 41–104 (2005).

[10] J. H. Duyn, "The future of ultra-high field MRI and fMRI for study of the human brain," NeuroImage **62**, 1241–1248 (2012).

[11] O. Kraff and H. H. Quick, "7T: Physics, safety, and potential clinical applications," J. Magn. Reson. Imaging **46**, 1573–1589 (2017).

[12] G. Barisano, F. Sepehrband, S. Ma, K. Jann, R. Cabeen, D. J. Wang, A. W. Toga, and M. Law, "Clinical 7 T MRI: Are we there yet? A review about magnetic resonance imaging at ultra-high field," Br. J. Radiol. **92**, 20180492 (2019).

[13] T. Nakada, "Clinical application of high and ultra high-field MRI," Brain Dev. **29**, 325–335 (2007).

[14] L. Frullano and T. J. Meade, "Multimodal MRI contrast agents," J. Biol. Inorg. Chem. **12**, 939–949 (2007).

[15] P. Fries, J. N. Morelli, F. Lux, O. Tillement, G. Schneider, and A. Buecker, "The issues and tentative solutions for contrast-enhanced magnetic resonance imaging at ultra-high field strength," Wiley Interdiscip. Rev.: Nanomed. Nanobiotechnol. **6**, 559–573 (2014).

[16] J. Wahsner, E. M. Gale, A. Rodríguez-Rodríguez, and P. Caravan, "Chemistry of MRI contrast agents: Current challenges and new frontiers," Chem. Rev. **119**, 957–1057 (2019).

[17] J. Garcia, J. Neelavalli, E. M. Haacke, and M. J. Allen, "Eu^{II}-containing cryptates as contrast agents for ultra-high field strength magnetic resonance imaging," Chem. Commun. **47**, 12858–12860 (2011).

[18] J. Garcia, A. N. W. Kuda-Wedagedara, and M. J. Allen, "Physical properties of Eu^{2+}-containing cryptates as contrast agents for ultrahigh-field magnetic resonance imaging," Eur. J. Inorg. Chem. **2012**, 2135–2140.

[19] L. Vander Elst, A. Roch, P. Gillis, S. Laurent, F. Botteman, J. W. M. Bulte, and R. N. Muller, "Dy-DTPA derivatives as relaxation agents for very high field MRI: The beneficial effect of slow water exchange on the transverse relaxivities," Magn. Reson. Med. **47**, 1121–1130 (2002).

[20] S. Aime, M. Botta, L. Barbero, F. Uggeri, and F. Fedeli, "Water signal suppression by T_2-relaxation enhancement promoted by Dy(III) complexes," Magn. Reson. Chem. **29**, S85–S88 (1991).

[21] M. Gueron, "Nuclear relaxation in macromolecules by paramagnetic ions: A novel mechanism," J. Magn. Reson. **19**, 58–66 (1975).

[22] I. Bertini, F. Capozzi, C. Luchinat, G. Nicastro, and Z. Xia, "Water proton relaxation for some lanthanide aqua ions in solution," J. Phys. Chem. **97**, 6351–6354 (1993).

[23] P. H. Fries and E. Belorizky, "Quantitative interpretation of the very fast electronic relaxation of most Ln^{3+} ions in dissolved complexes," J. Chem. Phys. **136**, 074513 (2012).

[24] M. Botta, F. Carniato, D. Esteban-Gómez, C. Platas-Iglesias, and L. Tei, "Mn(II) compounds as an alternative to Gd-based MRI probes," Future Med. Chem. **11**, 1461–1483 (2019).

[25] R. Sharp, "The mechanism of paramagnetic NMR relaxation produced by Mn(II): Role of orthorhombic and fourth-order zero field splitting terms," J. Chem. Phys. **129**, 144307 (2008).

[26] K. R. Lata, N. Sahoo, and T. P. Das, "Nature of second hydration shell in Mn^{+2}-aquoion system: Influence on proton relaxivity in nuclear magnetic resonance," J. Chem. Phys. **94**, 3715–3721 (1991).

[27] V. L. Ermolaev and E. B. Sveshnikova, "The application of luminescence-kinetic methods in the study of the formation of lanthanide ion complexes in solution," Russ. Chem. Rev. **63**, 905–922 (1994).

[28] K. J. H. Allen, E. C. Nicholls-Allison, K. R. D. Johnson, R. S. Nirwan, D. J. Berg, D. Wester, and B. Twamley, "Lanthanide complexes of the Kläui metalloligand, CpCo(P=O(OR)$_2$)$_3$: An examination of ligand exchange kinetics between isotopomers by electrospray mass spectrometry," Inorg. Chem. **51**, 12436–12443 (2012).

[29] H. Terraschke, M. Rothe, and P. Lindenberg, "*In situ* monitoring metal-ligand exchange processes by optical spectroscopy and X-ray diffraction analysis: A review," Rev. Anal. Chem. **37**, 20170003 (2018).

[30] L. Tei, Z. Baranyai, L. Gaino, A. Forgács, A. Vágner, and M. Botta, "Thermodynamic stability, kinetic inertness and relaxometric properties of monoamide derivatives of lanthanide(III) DOTA complexes," Dalton Trans. **44**, 5467–5478 (2015).

[31] M. Briganti, E. Lucaccini, L. Chelazzi, S. Ciattini, L. Sorace, R. Sessoli, F. Totti, and M. Perfetti, "Magnetic anisotropy trends along a full 4f-series: The f^{n+7} effect," J. Am. Chem. Soc. **143**, 8108–8115 (2021).

[32] J. A. Peters, J. Huskens, and D. J. Raber, "Lanthanide induced shifts and relaxation rate enhancements," Prog. Nucl. Magn. Reson. Spectrosc. **28**, 283–350 (1996).

[33] J. Kowalewski, C. Luchinat, T. Nilsson, and G. Parigi, "Nuclear spin relaxation in paramagnetic systems: Electron spin relaxation effects under near-redfield limit conditions and beyond," J. Phys. Chem. A **106**, 7376–7382 (2002).

[34] P. Gillis, A. Roch, and R. A. Brooks, "Corrected equations for susceptibility-induced T_2-shortening," J. Magn. Reson. **137**, 402–407 (1999).

[35] M.-E. Boulon, G. Cucinotta, J. Luzon, C. Degl'Innocenti, M. Perfetti, K. Bernot, G. Calvez, A. Caneschi, and R. Sessoli, "Magnetic anisotropy and spin-parity effect along the series of lanthanide complexes with DOTA," Angew. Chem., Int. Ed. **52**, 350–354 (2013).

[36] F. Benetollo, G. Bombieri, S. Aime, and M. Botta, "A holmium complex of a macrocyclic ligand (DOTA) and its isostructural europium analogue," Acta Crystallogr., Sect. C: Cryst. Struct. Commun. **55**, 353–356 (1999).

[37] J. F. Desreux, "Nuclear magnetic resonance spectroscopy of lanthanide complexes with a tetraacetic tetraaza macrocycle. Unusual conformation properties," Inorg. Chem. **19**, 1319–1324 (1980).

[38] R. W. Brown, Y.-C. N. Cheng, E. M. Haacke, M. R. Thompson, and R. Venkatesan, *Magnetic Resonance Imaging: Physical Principles and Sequence Design* (John Wiley & Sons, 2014).

[39] E. Anoardo, G. Galli, and G. Ferrante, "Fast-field-cycling NMR: Applications and instrumentation," Appl. Magn. Reson. **20**, 365–404 (2001).

[40] C. V. G. Ferrante, D. Canina, E. Bonardi, M. Polello, and P. Golzi, "Measurement of spin-spin relaxation time T_2 at very low magnetic field by means of the fast field cycling NMR method," in 48th ENC Conference, 2007.

[41] D. Esteban-Gómez, C. Cassino, M. Botta, and C. Platas-Iglesias, "^{17}O and ^{1}H relaxometric and DFT study of hyperfine coupling constants in [Mn(H$_2$O)$_6$]$^{2+}$," RSC Adv. **4**, 7094–7103 (2014).

[42] D. H. Powell, O. M. N. Dhubhghaill, D. Pubanz, L. Helm, Y. S. Lebedev, W. Schlaepfer, and A. E. Merbach, "Structural and dynamic parameters obtained from

^{17}O NMR, EPR, and NMRD studies of monomeric and dimeric Gd^{3+} complexes of interest in magnetic resonance imaging: An integrated and theoretically self-consistent approach," J. Am. Chem. Soc. **118**, 9333–9346 (1996).

[43] K. Micskei, L. Helm, E. Brücher, and A. E. Merbach, "^{17}O NMR study of water exchange on [Gd(DTPA)(H$_2$O)]$^{2-}$ and [Gd(DOTA)(H$_2$O)]$^-$ related to NMR imaging," Inorg. Chem. **32**, 3844–3850 (1993).

[44] G. González, D. H. Powell, V. Tissières, and A. E. Merbach, "Water-exchange, electronic relaxation, and rotational dynamics of the MRI contrast agent [Gd(DTPA-BMA)(H$_2$O)] in aqueous solution: A variable pressure, temperature, and magnetic field ^{17}O NMR study," J. Phys. Chem. **98**, 53–59 (1994).

[45] I. Bertini, C. Luchinat, and G. Parigi, "^{1}H NMRD profiles of paramagnetic complexes and metalloproteins," Adv. Inorg. Chem. **57**, 105–172 (2005).

[46] R. Hausser and F. Noack, "Kernmagnetische relaxation und korrelation in zwei-spin-systemen," Z. Phys. **182**, 93–110 (1964).

[47] I. Bertini, F. Briganti, Z. C. Xia, and C. Luchinat, "Nuclear magnetic relaxation dispersion studies of hexaaquo Mn(II) ions in water-glycerol mixtures," J. Magn. Reson., Ser. A **101**, 198–201 (1993).

[48] S. Aime, M. Botta, G. Ermondi, F. Fedeli, and F. Uggeri, "Synthesis and NMRD studies of gadolinium(3+) complexes of macrocyclic polyamino polycarboxylic ligands bearing β-benzyloxy-α-propionic residues," Inorg. Chem. **31**, 1100–1103 (1992).

[49] S. Aime, L. Barbero, M. Botta, and G. Ermondi, "Determination of metal-proton distances and electronic relaxation times in lanthanide complexes by nuclear magnetic resonance spectroscopy," J. Chem. Soc., Dalton Trans. **1992**, 225–228.

[50] R. Marin, G. Brunet, and M. Murugesu, "Shining new light on multifunctional lanthanide single-molecule magnets," Angew. Chem., Int. Ed. **60**, 1728–1746 (2021).

[51] E. Terreno, P. Boniforte, M. Botta, F. Fedeli, L. Milone, A. Mortillaro, and S. Aime, "The water-exchange rate in neutral heptadentate DO3A-like Gd^{III} complexes: Effect of the basicity at the macrocyclic nitrogen site," Eur. J. Inorg. Chem. **2003**, 3530–3533.

[52] G. Cucinotta, M. Perfetti, J. Luzon, M. Etienne, P.-E. Car, A. Caneschi, G. Calvez, K. Bernot, and R. Sessoli, "Magnetic anisotropy in a dysprosium/DOTA single-molecule magnet: Beyond simple magneto-structural correlations," Angew. Chem., Int. Ed. **51**, 1606–1610 (2012).

[53] E. A. Suturina, K. Mason, C. F. G. C. Geraldes, N. F. Chilton, D. Parker, and I. Kuprov, "Lanthanide-induced relaxation anisotropy," Phys. Chem. Chem. Phys. **20**, 17676–17686 (2018).

[54] L. Smentek, B. Andes Hess, J. P. Cross, H. Charles Manning, and D. J. Bornhop, "Density-functional theory structures of 1,4,7,10-tetraazacyclododecane-1,4,7,10-tetraacetic acid complexes for ions across the lanthanide series," J. Chem. Phys. **123**, 244302 (2005).

[55] J. W. M. Bulte, C. Wu, M. W. Brechbiel, R. A. Brooks, J. Vymazal, M. Holla, and J. A. Frank, "Dysprosium-DOTA-PAMAM dendrimers as macromolecular T$_2$ contrast agents: Preparation and relaxometry," Invest. Radiol. **33**, 841–845 (1998).

[56] K. E. Kellar, S. L. Fossheim, and S. H. Koenig, "Magnetic field dependence of solvent proton relaxation by solute dysprosium(III) complexes," Invest. Radiol. **33**, 835–840 (1998).

[57] In the literature, the value of $\Delta = E/\hbar$ is usually expressed in frequency unit (s^{-1}).